Sensors & Actuators: A. Physical 390 (2025) 116587

Contents lists available at ScienceDirect

Sensors and Actuators: A. Physical

journal homepage: www.journals.elsevier.com/sensors-and-actuators-a-physical

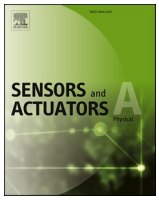

Resonance frequency measurement for space accelerometer

Didier Chérubin Negretto [a,*], Jan ten Pierick [a], Luigi Ferraioli [a], Daniel Bieri [a], Pierrick Cheiney [b], Olivier Jolly [b], Domenico Giardini [a]

[a] Institute for Geophysics, ETH Zürich, Sonneggstrasse 5, Zürich 8092, Switzerland
[b] Exail, Rue Paul Sabatier 2, Lannion 22300, France

ARTICLE INFO

Keywords:
Resonance frequency
Accelerometer
Phase noise
Stray capacitance compensation

ABSTRACT

Resonance frequency measurements are used for various applications: atomic force microscopes, mass detection, biochemical and inertial sensors. In this article a detailed analysis of the performances of a resonance frequency measurement method are presented and demonstrated using a space grade accelerometer. The method consists of replacing the feedback of the oscillator with a controller that drives the sensor's input, acquires the sensor's output, determines the phase shift between the sensor's input and output, converts it to a resonance frequency measurement and adjusts the drive signal's frequency. The innovative phase to frequency conversion model used ensures a fast convergence of the drive signal towards the resonance frequency. The maximum measured relative error while searching for the resonance frequency is of 0.04 [%]. The tracking of the resonance frequency shows no oscillations or overshoots because the resonance frequency is exactly measured. The achieved measurement noise floor for the specific sensor used is 0.13 $[mHz/\sqrt{Hz}]$ at 1 $[Hz]$. The measurement method presented can be exploited for other applications which also rely on the measurement of the resonance frequency of a piezo-electric resonator.

1. Introduction

Measuring the resonance frequency is used for many applications including: atomic force microscopes [1], mass detection [2], inertial sensors [3,4] and the detection of biological and chemical substances [5]. This article presents the electrical circuit and data processing algorithm used to acquire the resonance frequency of a Micro Electro Mechanical System (MEMS) accelerometer [6,7] for space applications.

The measurement of the resonance frequency is not a straightforward operation. It requires, in fact, the following functions: exciting the sensor, acquiring the output signal and processing the data. For each of these functions different implementations have been tested in literature.

The two main solutions to drive the sensor are the self-sustained oscillator [1,8] and the digital feedback oscillator [9]. The self-sustained oscillator relies on an analog feedback loop which keeps the sensor at resonance. The analog feedback may include an Automatic Gain Control (AGC) circuit to limit the amplitude of the excitation signal otherwise the crystal is overdriven.

The digital feedback oscillator does not require an AGC and it does not overdrive the crystal. Because the system has control over the drive signal, it can measure the transfer function of the sensor. From the transfer function the system can determine the internal parameters of the sensor. The values of the internal parameters can then be tracked over time or in different conditions to verify that the sensor is always operating within specifications.

Concerning the acquisition, the output sense signal is usually measured using an Analog to Digital Converter (ADC) [9,10] or a comparator [11–13]. The ADC makes it possible to sample the signal at a fixed sampling frequency. The sampling frequency can be synchronized with other instruments, thus simplifying the comparison of data from different sources. Furthermore, the ADC provides information on the amplitude of the sense signal, which can be used to determine if the sensor is operating correctly (e.g.: if the amplitude drops, the sensor might be damaged and the measurement un-reliable). The comparator method requires less components and power, yet at the cost of an irregular sampling rate and lack of amplitude information.

The data processing strongly depends on the acquisition method selected. With the comparator one can, for example, make a time-to-

Abbreviations: ADC, Analog to Digital Converter; DAC, Digital to Analog Converter; FIR, Finite Impulse Response; LIA, Lock-In Amplifier; LUT, Look-Up Table; MEMS, Micro Electro Mechanical System; PID, Proportional Integrative Derivative; AGC, Automatic Gain Control.

* Corresponding author.
E-mail address: didier.negretto@eaps.ethz.ch (D.C. Negretto).

https://doi.org/10.1016/j.sna.2025.116587
Received 13 September 2024; Received in revised form 27 March 2025; Accepted 13 April 2025
Available online 17 April 2025

digital converter, count the number of cycles in a given time interval or interpolate the input values to obtain a fixed sampling rate. If the ADC is used a demodulation algorithm may be used instead. If the self-sustained oscillator is adopted there is no need for a signal generator to drive the sensor, which is mandatory if the digital feedback oscillator is used. Discussing all the possible implementations is beyond the scope of this article, the focus is placed on the implemented solution, which consists of a digital feedback oscillator using an ADC.

For the sensor studied in this article different comparator-based strategies have been applied to measure the acceleration [11,12]. A theoretical analysis of different measurement architectures has been performed [14,15]. Some aspects of the design, such as the stray capacitance compensation [16,17], noise [18] and data processing [10] was analysed in previous literature.

This article complements the theoretical analysis by describing the hardware design, explains what are the requirements to find and track the resonance frequency using a digital feedback loop and shows how the different parts of the measurement method impact the measurement's properties providing a valuable overview of the system.

The method used for this study relies on an ADC for the acquisition and on a digital feedback oscillator architecture to drive the sensor and track the resonance frequency. The accelerometer is designed such that the resonance frequency of the device changes proportionally to the applied acceleration [19]. The sensor is driven using a sinusoidal signal to measure the resonance frequency.

The complex impedance of the sensor introduces a phase shift φ between the input of the device and the output. The phase shift is measured and converted to the difference between the resonance frequency and the drive frequency $\Delta\omega = \omega_s - \omega_d$, where $\Delta\omega$ is the error, ω_s is the resonance frequency and ω_d is the drive frequency.

The conversion is achieved using a model of the sensor. The model is created during self-initialisation by measuring for each value of φ, the corresponding $\Delta\omega$ value and storing it in memory. The error information is used to keep the sensor at resonance using a feedback loop.

This article is structured as follows: Section 2 presents the theory of the measurement and of the data processing, Section 3 briefly explains the test setup used for the measurements, Section 4 illustrates and discuss the results obtained and Section 5 provides final remarks and conclusions.

2. Theoretical analysis

In this section the analog design is described first, then the algorithm to acquire the data is presented. The analog design describes the stray capacitance compensation and the analog amplification. The algorithm section explains how φ is computed, how the φ to $\Delta\omega$ conversion is done, how ω_s is determined and how the feedback loop is closed.

Fig. 2–1 shows the sensor's electrical model as well as the electronic circuit used to amplify the output signal of the sensor. The sensor model consists of the motional parameters R_m, C_m and L_m and of the stray capacitance C_0. The motional parameters define the resonance frequency $\omega_s = 1/\sqrt{C_m L_m}$ and the quality factor $Q = L_m\omega_s/R_m$ of the sensor.

2.1. Analog electronics

The sensor has an unwanted stray capacitance, through which flows the current i_{par}. This current causes a phase shift [16,17], which inhibits the measurement for $\omega_d > \omega_s$, hence the need to reduce or ideally remove i_{par}. This is done using the stray capacitance compensation circuit, which creates the current i_{comp}, such that $i_{par} + i_{comp} \approx 0$.

Solving the circuit in Fig. 2–1, yield to Eq. (2–1), under the assumption that the input current of the amplifier is negligible.

$$\begin{aligned} i_{tot} &= i_m + i_{par} + i_{comp} \\ &= \frac{V_{drive} - V_{ninv}}{Z_m} + (V_{drive} - V_{ninv}) * sC_0 + \left(-\frac{V_{drive}}{a} - V_{ninv} \right) * sC_{comp} \end{aligned} \tag{2-1}$$

Where a is the attenuation of the resistive divider made by R_{div1} and R_{div2}. Given that V_{drive} has a much higher amplitude than V_{ninv} it is possible to assume that $V_{drive} - V_{ninv} \approx V_{drive}$ and $-V_{drive} - V_{ninv} \approx V_{drive}$. This results in Eq. (2–2):

$$i_{tot} = \frac{V_{drive}}{Z_m} + V_{drive} * sC_0 - \frac{V_{drive}}{a} * sC_{comp} = V_{drive} * \left(\frac{1}{Z_m} + s\left(C_0 - \frac{C_{comp}}{a} \right) \right) \tag{2-2}$$

Once the compensation circuit is appropriately tuned by selecting $a = (R_{div1} + R_{div2})/R_{div2}$, then the residual stray capacitance $C_0' = C_0 - C_{comp}/a \approx 0$. This assumption yields to Eq. (2–3) where ω_d is the frequency of the drive signal V_{drive}.

$$\frac{i_{tot}}{V_{drive}} = \frac{1}{Z_m} = \frac{1}{\frac{1}{sC_m} + sL_m + R_m} = \frac{\frac{s}{L_m}}{s^2 + \frac{R_m}{L_m}s + \frac{1}{L_m C_m}} = \frac{\frac{\omega_d^2 R_m}{L_m^2} + \frac{j\omega_d}{L_m}\left(\frac{1}{L_m C_m} - \omega_d^2\right)}{\left(\frac{1}{L_m C_m} - \omega_d^2\right)^2 + \frac{\omega_d^2 R_m^2}{L_m^2}} \tag{2-3}$$

The goal of the analog amplification is to convert the current output

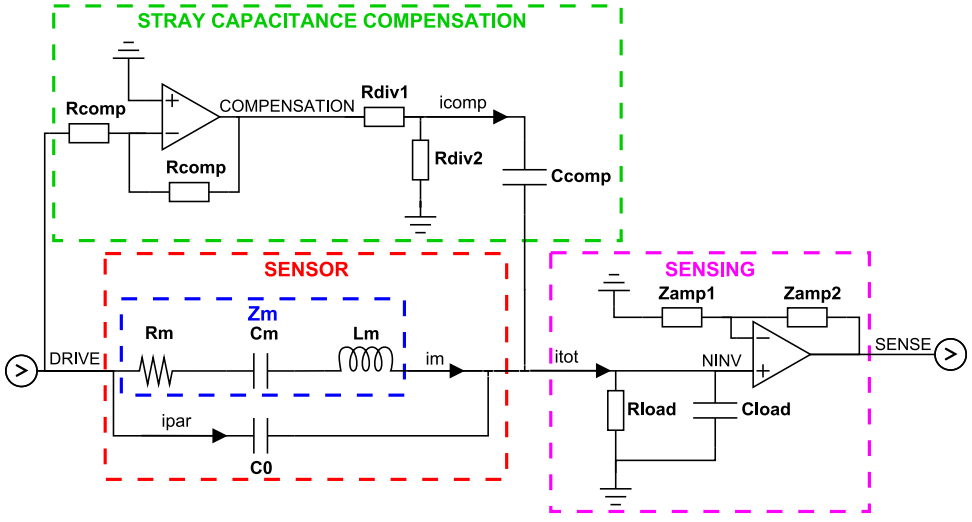

Fig. 2-1. Sensor model including sensing and compensation circuit.

of the sensor in an amplified voltage that can then be acquired and treated by the digital feedback loop.

Knowing the load impedance $Z_{load} = R_{load}/(1 + j\omega_d R_{load} C_{load})$ and the bandpass gain of the amplifier A, it is possible to write Eq. (2–4).

$$V_{sense} = A * V_{ninv} = A * Z_{load} * i_{tot} = A * Z_{load} * \frac{\frac{\omega_d^2 R_m}{L_m^2} + \frac{j\omega_d}{L_m}\left(\omega_s^2 - \omega_d^2\right)}{\left(\omega_s^2 - \omega_d^2\right)^2 + \frac{\omega_d^2 R_m^2}{L_m^2}} * V_{drive} \tag{2-4}$$

The stray capacitance compensation circuit, the load impedance and the amplifier are designed to add a constant phase shift φ_{amp} over the operating frequency range of the sensor.

2.2. Digital feedback

Fig. 2–2 presents the measurement method and the feedback loop for the sensor. The algorithm is presented starting from the output signal of the sensor, which is sampled, demodulated, filtered, converted to a resonance frequency measurement and then used to correct the drive frequency of the sensor.

The sensor output signal is sampled at a frequency higher than double its maximum resonance frequency using an ADC. After sampling, the data is demodulated, this is accomplished by multiplying the samples with $\sin(\theta)$ and $\cos(\theta)$, where θ is the value of the phase used to create the drive signal at the moment the sample is taken. The sine and cosine values are called Y and X respectively. Using θ for the demodulation ensures that the signal from the sensor is always demodulated with the correct frequency, which corresponds to ω_d.

After demodulation the X and Y signals are filtered using a low-pass Finite Impulse Response (FIR) filter. The filter removes the unwanted signal at double the drive frequency and reduces the bandwidth to the measurement bandwidth ω_{meas}. Because the high frequency content of the signal is removed by the FIR filter, X and Y can be down-sampled.

The down-sampled X and Y values are used to compute the power and phase φ of the acquired signal. The power can be used as a housekeeping measurement, to show that the sensor is in resonance.

The phase can be converted to a resonance frequency measurement using one of the three main options available: the linear model, the theoretical sensor model and the measured sensor model. The linear model is the simplest, but it is only accurate in a small frequency around resonance (as shown in Fig. 4–1). The theoretical model is more accurate, but with a similar computational power it is possible to use the measured sensor model, which is the most accurate.

Another advantage of the measured sensor model is that the φ to $\Delta\omega$ Look-Up Table (LUT) can be updated and measured remotely. Access to this information can be used in production, testing and to understand possible issues remotely once the solution is deployed. For example, if the quality factor decreases over time, this might be a sign of a leak in the packaging of the sensor or of ageing of the crystal. During testing this can lead to discarding the sensor, while if the same issue is faced after deployment the φ to $\Delta\omega$ LUT can be updated to keep using the sensor although with a reduced performance.

The LUT is created during a self-initialisation procedure, which consists of measuring for each $\Delta\omega = \omega_s - \omega_d$ the value of φ and storing the results in memory. The self-initialisation is done while the sensor is in a static environment. During the subsequent measurements the value of φ is converted to $\Delta\omega$ using the data stored in memory and then ω_s is computed using $\omega_s = \Delta\omega + \omega_d$.

As explained in Refs. [1,14,15] the sensor has a limited bandwidth, given by $\omega_{BW} = \omega_s/2Q$. In practice if only the φ to $\Delta\omega$ LUT is used, the bandwidth of the measurement is limited to ω_{BW}. Because of the high quality factor Q of MEMS sensors we can assume that $\omega_{meas} > \omega_{BW}$. The system is designed such that for every φ measured ω_d is updated (i.e. the loop frequency is equal to ω_{meas}). The digital controller can therefore react faster to resonance frequency changes than the sensor, thus ensuring that resonance is always maintained.

The bandwidth limitation can be overcome by adding the derivative of φ over time $d\varphi/dt$ to the measured resonance frequency ω_s, thus obtaining $\omega_s' = \omega_d + \Delta\omega + d\varphi/dt$. To understand how this bandwidth increase works, let's suppose that $\omega_s = \omega_d = constant$, then $\Delta\omega = d\varphi/dt = 0$. If the resonance frequency changes abruptly, then $\Delta\omega$ will slowly change (limited by ω_{BW}), while $d\varphi/dt$ will be rather large right after the change and will decrease as ω_d converges to the new ω_s. $d\varphi/dt$ helps therefore capturing the sudden change in resonance frequency, but it comes with a noise increase, as explained in Section 4.4.

To close the feedback loop, $\Delta\omega$ is used in a Proportional Integral and Derivative (PID) controller, which applies a correction to the drive frequency to bring it closer to the resonance frequency of the sensor $\omega_d(t) = \omega_d(t-1) + K_i * \Delta\omega$. The PID controller keeps the drive frequency as close as possible to the resonance frequency of the sensor even if the resonance frequency changes over time. This ensures that the lowest noise is obtained.

When using an appropriate model for the φ to $\Delta\omega$ LUT an integrative controller with a constant lower than 1 is enough to find and track the resonance frequency of the sensor without oscillations or overshoots. Using a constant just below 1 ensures that the loop does not become unstable.

The last step of the algorithm is the creation of the drive signal. This is achieved using the phase accumulator, which updates the phase of the drive signal θ using the current value of the drive frequency computed by the PID controller $\theta(t) = \theta(t-1) + \omega_d * dt$. The phase is then converted to an amplitude value using the sine LUT and modulated to create

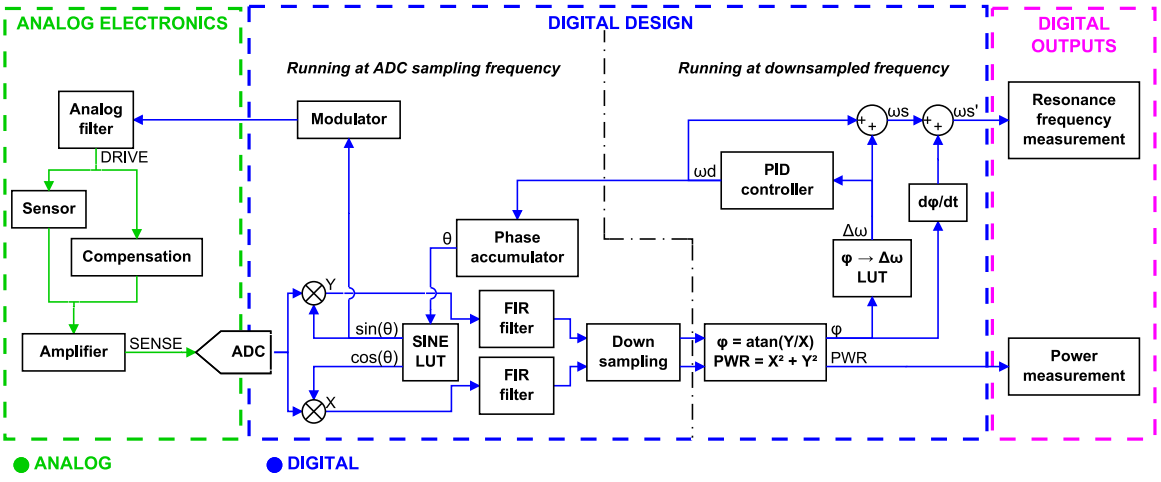

Fig. 2–2. Measurement algorithm.

an analog voltage. The modulation can be implemented digitally in the programmable device or using an external Digital to Analog Converter (DAC).

3. Test setup

Fig. 3–1 shows the test setup used to acquire the data from the accelerometer. The Lock-In Amplifier (LIA) performs the sampling, demodulation and down-sampling of the sense signal from its input port. It provides the FIR-filtered X and Y values to the computer, where they are then treated and used to perform the measurement.

Three programs are used to control the LIA: for the transfer function test (see Section 4.1) the LIA performs a frequency sweep, for the convergence and tracking tests (see Sections 4.2 and 4.3) the LIA tracks the resonance frequency using the algorithm described in Section 2.2 and finally for the noise measurement (see Section 4.4) the LIA drives the sensor at resonance, keeping a constant drive frequency.

One can notice that in the test setup the compensation signal is controlled by the LIA, while the drive signal is the inverted copy of the compensation signal, this is due to a limitation of the prototype. A phase shift of -180 [deg] is applied to make the results equal to the ones of the final implementation, more understandable and easier to compare with literature.

Different tests are performed using the same test setup. The first one consists of the measurement of the transfer function of the sensor. The data of the transfer function of the sensor is then used to implement the φ to $\Delta\omega$ LUT for the later tests. The second test shows that it is possible for the system to efficiently find the resonance frequency of the sensor within a wide frequency range. The third test is used to show that the controller is able to track the resonance frequency of the sensor and that the results match with the expected values. Finally, the noise of the measurement is presented and the different noise contributions are analysed.

4. Results

In this section the results from the tests are presented and discussed. Section 4.1 presents the measurement of the transfer function, Section 4.2 shows that the proposed method is capable of finding the resonance frequency, Section 4.3 deals with the tracking behaviour, and Section 4.4 analyses the noise performance.

4.1. Transfer function measurement

The goal of this measurement is to show that the measured transfer function of the sensor and the theoretical model derived from Eq. (2–4) coincide within the assumptions made for the model. The transfer function is measured using the test setup presented in Fig. 3–1.

The LIA is programmed to find the resonance frequency ω_s and then measure the X and Y values in a 400 [Hz] range around it. This range corresponds to the measurement range of the sensor. The X and Y values are then processed to compute the amplitude and phase of the transfer function.

Fig. 4–1 compares the measured transfer function with the theoretical model. A phase shift of -99.8 [deg] is added to the model to account for the phase shift φ_{amp} introduced by the sensing amplifier and the stray capacitance compensation circuit (see Section 2.1).

One can notice that at frequencies higher than the resonance frequency of 63702 [Hz], the model and the measured phase and amplitude start to diverge. This is because of the residual stray capacitance C_0', which starts to have an effect at higher frequencies.

These results show that the theoretical model and the measurement coincide rather well near the resonance frequency, but that they diverge because of the residual stray capacitance.

4.2. Convergence test

The convergence test shows that the proposed method converges to the correct resonance frequency measurement even when the initial $\Delta\omega$ is large. To prove this the φ to $\Delta\omega$ LUT is created using the data measured during the previous experiment. The initial drive frequency is set to $\omega_d(t=0) = \omega_s + \Delta\Omega$, with $\Delta\Omega = \pm 200$ [Hz], the algorithm is then run and data are collected. The value of $\Delta\Omega = \pm 200$ [Hz] corresponds to the measurement range of the sensor used for the tests.

The algorithm is able to converge towards the expected value for the two tested cases. Fig. 4–2 shows that the method is able to determine the resonance frequency with an error smaller than 1 [Hz] after only five updates of the drive frequency.

This measurement shows that the proposed φ to $\Delta\omega$ LUT works as intended. The upper part of Fig. 4-2 compares the measurement results in green with the drive frequency in red. One can immediately notice that the green lines, to which the $\Delta\omega$ correction from the LUT is added, are much closer to the final result than the red ones. This means that the

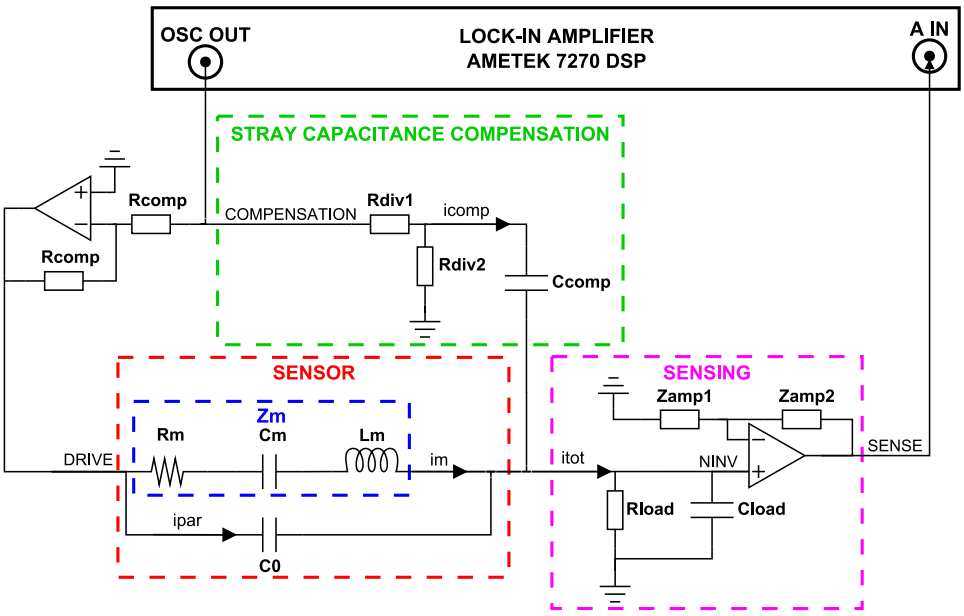

Fig. 3–1. Measurement test setup.

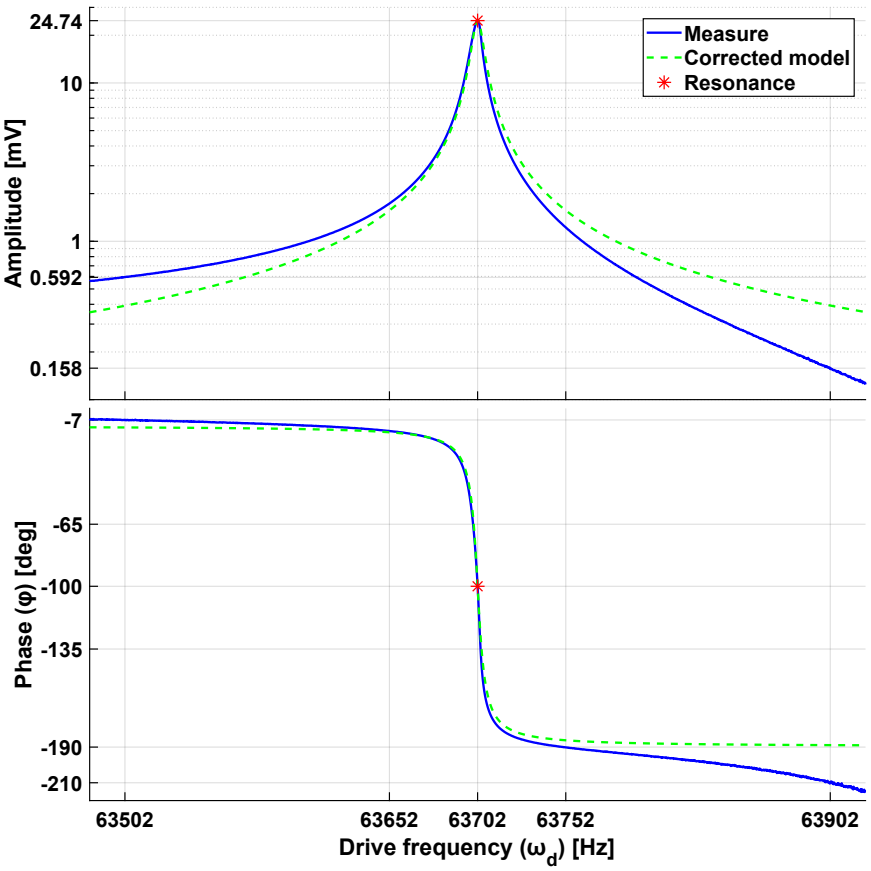

Fig. 4–1. Sensor model and measurement compared.

proposed method is capable of accurately measure the resonance frequency even if the steady state is not reached yet.

The maximum measurement error, which occurs at the start of the measurement, is below 0.04 [%], while the drive frequency has an error of 0.3 [%]. The proposed model reduces the relative error of the measurement by almost one order of magnitude. For the sensor tested in this article the system is accurate when powered up and quickly converges to the resonance frequency.

The feedback loop is capable of reaching the setpoint without oscillations or overshoots. This is ensured by design: $\Delta\omega$ is based on the properties of the specific sensor and therefore the resonance frequency is always computed exactly.

For this test the integrative coefficient K_i of the PID controller is set to 0.9, while the proportional K_p and derivative coefficients K_d are set to 0. The controller is stable as long as K_i is < 1 and $K_p = K_d = 0$.

One can notice that the sampling rate is rather low. This limitation is a consequence of the test setup and can easily be fixed by implementing the algorithm in a programmable device. Because of the low sampling rate, the $d\varphi/dt$ is not used for computing the resonance frequency. This has no impact on the result because the value of $d\varphi/dt$ is not used by the PID controller.

4.3. Tracking performance

During the tracking test the sensor is mounted on a tilting support, such that the orientation of the sensitive axis of the sensor with respect to gravity can be changed. The sensor is tilted in three different positions: left, up and down. In the left position the measured acceleration is between $-1[g]$ and $+1$ $[g]$, but not zero due to a mechanical limitation of the tilting support. In the face up position an acceleration of $+1[g]$ is measured and in the face down position and acceleration of $-1[g]$ is measured. This test is not designed to measure the linearity of the sensor (test results for the sensor used in this article are already available in Ref. [19]).

The test is divided in two phases: during the first phase the resonance frequency of the sensor is tracked while the sensor is moved into the three positions (green line on the left of Fig. 4–3), during the second phase the sensor is locked in the three positions, while the transfer function is measured (right side of Fig. 4–3).

Fig. 4–3 shows on the left the time series of the first measurement and on the right the transfer function of the sensor for comparison. One can notice that the resonance frequency measured with the suggested method matches well with the resonance frequency measured using the transfer function, as expected.

The sensor used for this test is different than the one used for the measurements presented in the previous sections, hence why the transfer function is not identical. This also shows the importance of the self-initialisation procedure, which ensures that the differences between the sensors are corrected by the algorithm.

4.4. Noise performance

This test shows the performance of the proposed method in combination with the tested sensor and illustrates how the noise performance is affected by the limited bandwidth of the sensor.

Let's assume that the noise of the measured φ is white noise and that this white noise is at a level of $\mathcal{N}(\varphi)$. We can now compute the noise level after the $\varphi \rightarrow \Delta\omega$ LUT, $\mathcal{N}(\omega_s)_{LUT}$. Assuming the system is in a steady state with the sensor driven at resonance, we can use the linear approximation for the φ to $\Delta\omega$ LUT. $\mathcal{N}(\omega_s)_{LUT}$ can then be approximated with equation Eq. (4–1), where $K_{LUT} = 57.34 * 10^{-3}$ $[mHz/mdeg]$. $\mathcal{N}(\varphi)$ is measured to be $\mathcal{N}(\varphi) = 2.27$ $\left[mdeg/\sqrt{Hz}\right]$.

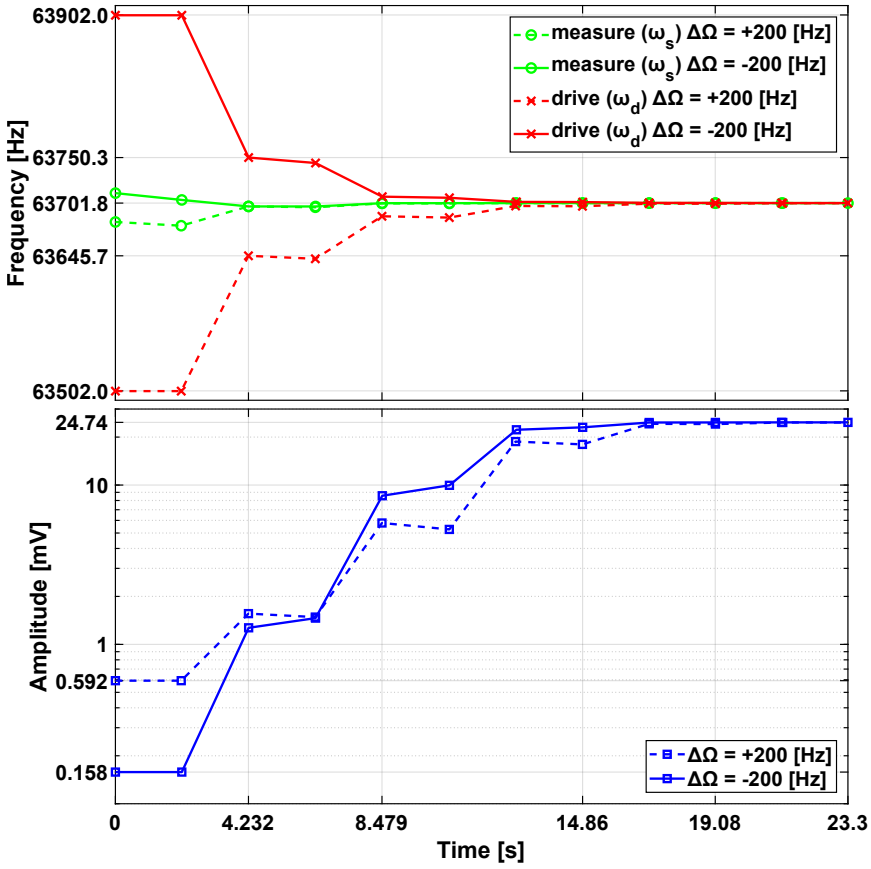

Fig. 4–2. Convergence test measurement.

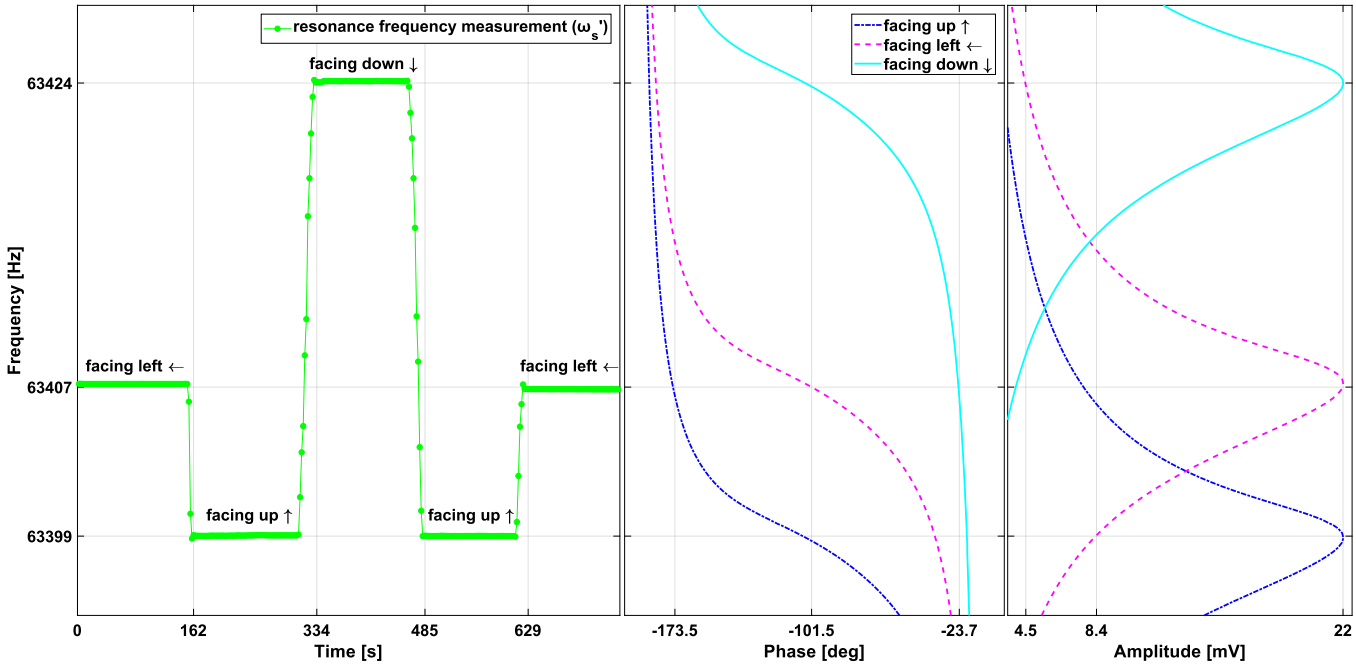

Fig. 4–3. Tracking test results.

$$\mathcal{N}(\omega_s)_{LUT} = \mathcal{N}(\varphi) * K_{LUT} \tag{4-1}$$

$\mathcal{N}(\omega_s)_{LUT}$ is expected to be constant over frequency, while the measured signal is filtered by the oscillator properties for frequencies above ω_{BW}. To compensate for the attenuation, the inverse of the transfer function of the sensor is applied to $\mathcal{N}(\omega_s)_{LUT}$. The total theoretical noise is given in Eq. (4–2), where $H_S = 1/(1 + j\omega/\omega_{BW})$ is the transfer function of the sensor.

$$\mathcal{N}(\omega_s) = \mathcal{N}(\varphi) * K_{LUT} * |1/H_S| = \mathcal{N}(\varphi) * K_{LUT} * \sqrt{1 + \left(\frac{\omega}{\omega_{BW}}\right)^2}$$
$$= \mathcal{N}(\varphi) * K_{LUT} * \sqrt{1 + \left(\frac{2Q}{\omega_s}\omega\right)^2} \quad (4\text{-}2)$$

Fig. 4–4 shows the resonance frequency noise measured using the algorithm presented in Section 2.2 compared to the simple model presented in equation Eq. (4–2). The model and the measurements are coherent. At low frequencies the noise starts to increase with respect to the model this is most likely due to ambient noise (e.g.: small movements of the test setup or changes in ambient temperature).

Fig. 4–5 shows $\mathcal{N}(\omega_s)_{LUT}$ and the noise contribution from $d\varphi/dt$, $\mathcal{N}(\omega_s)_{d\varphi/dt}$ separately. $\mathcal{N}(\omega_s)_{LUT}$ is dominant for low frequencies $< \omega_{BW}$ and $\mathcal{N}(\omega_s)_{d\varphi/dt}$ is the major noise contributor for high frequencies $> \omega_{BW}$. This is expected as $d\varphi/dt$ is used to increase the gain of the measurement at high frequencies.

To measure signals above ω_{BW} without attenuation, $d\varphi/dt$ must be added. Similarly, by only using $d\varphi/dt$ the signals at frequencies below ω_{BW} will be attenuated.

From these noise results it is possible to get a simple empirical intuition: the cause of the noise density increases above ω_{BW} appears to be the amplification required at high frequencies to counteract the low-pass behaviour of the sensor.

This effect is well document in literature [18] and the results from the measurements done in this article agree with previous results.

5. Conclusion

In this article a method to find, track and measure the resonance frequency of an oscillating system is presented. The proposed method is demonstrated using a MEMS space accelerometer. The accelerometer works by having a resonance frequency that changes proportionally to the acceleration applied to the sensor. The change of the resonance frequency causes a phase shift between the input and output of the sensor.

The proposed method uses the phase shift information for the measurement. The value of the resonance frequency is measured using a self-initialised look-up table that converts the phase shift into a resonance frequency measurement. The LUT accounts for the non-linearity of the phase to frequency conversion, which is generally not the case for other phase locked loop algorithms, thus providing accurate results even if the drive frequency differs from the resonance frequency. The proposed algorithm can find the resonance frequency within the measurement range without an initial guess and without scanning all the possible frequencies. The derivative of the phase shift is added to the converted value to increase the measurement bandwidth. This is needed to overcome the bandwidth limitation of the sensor.

The method converges to the correct resonance frequency in a few measurement samples and maintains resonance without overshoots or oscillations, ensuring optimal noise performance during measurement. The maximum measured relative error while searching for the resonance frequency in the measurement range of the sensor is of only 0.04 [%]. The measured noise floor for the sensor tested in this article is 0.13 $[mHz/\sqrt{Hz}]$ at 1 $[Hz]$.

This paper provides an empirical explanation of the noise shape, showing that the increase in noise density for frequencies above the bandwidth limit of the sensor is caused by the increased gain of the measurement required to compensate the attenuation introduced by the sensor. This intuition is in accordance with previous literature and theoretical analysis.

Future developments include the implementation of the software in a programmable device, such that the sampling rate limitations encountered using laboratory instrumentation can be overcome. During the implementation the effects of quantisation and systematic errors can be studied to obtain the maximum performance. This same measurement method can be exploited for other applications which also rely on the measurement of the resonance frequency of an oscillator.

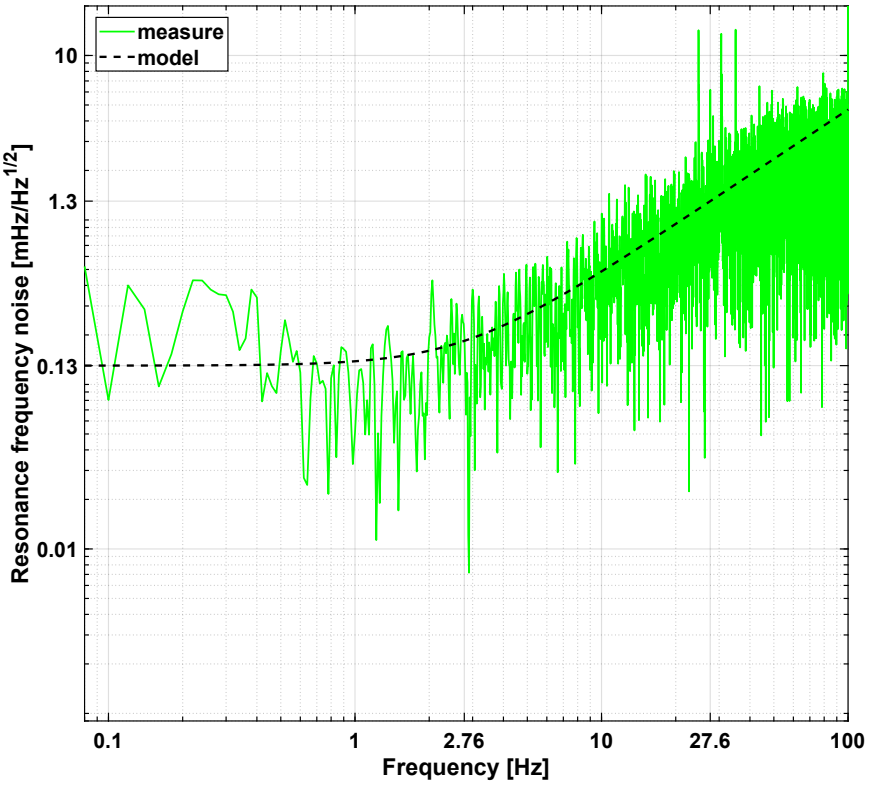

Fig. 4–4. Total measurement noise.

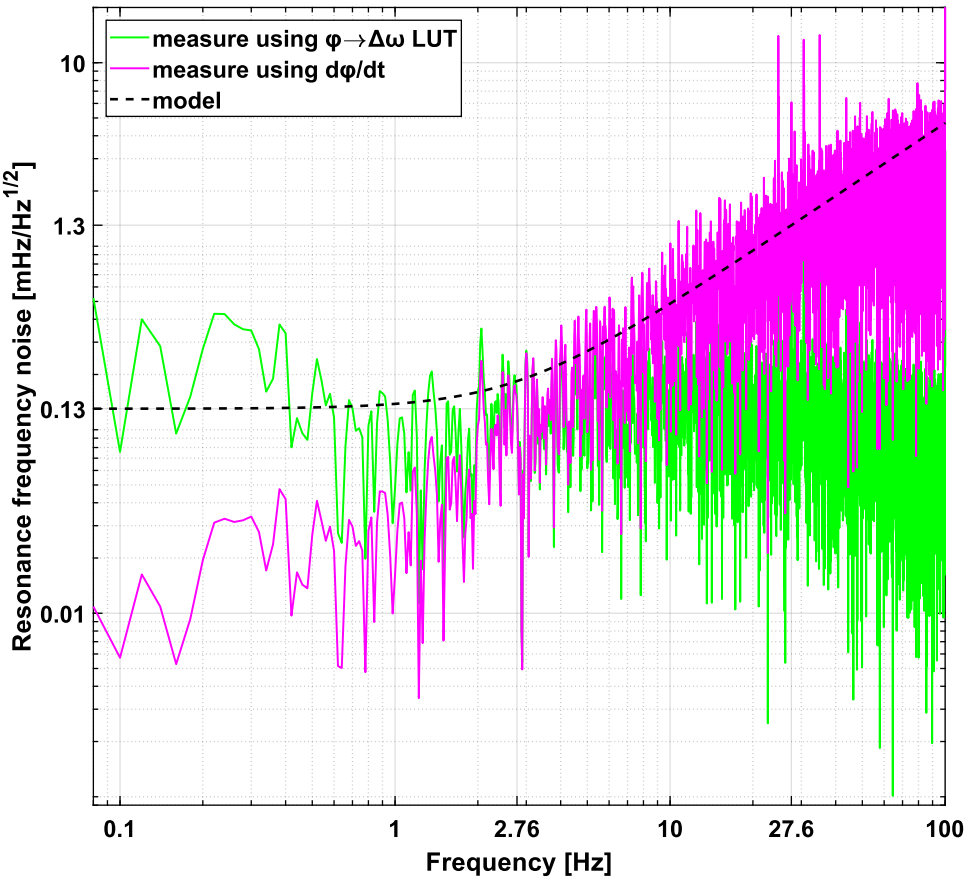

Fig. 4–5. Noise contributors.

The system can further be improved by giving control over the compensation signal's amplitude to the digital controller, so that the compensation signal can be tuned automatically and more precisely. This should lead to an easier tuning procedure and better stray capacitance compensation overall.

CRediT authorship contribution statement

Olivier Jolly: Writing – review & editing, Resources. **Pierrick Cheiney:** Writing – review & editing, Resources. **Daniel Bieri:** Validation. **Luigi Ferraioli:** Writing – review & editing, Validation, Supervision, Resources, Project administration, Funding acquisition. **Jan ten Pierick:** Writing – review & editing, Validation, Conceptualization. **Didier Chérubin Negretto:** Writing – original draft, Visualization, Software, Methodology, Investigation, Formal analysis, Data curation, Conceptualization. **Domenico Giardini:** Supervision, Project administration, Funding acquisition.

Funding sources

Funding: This work was supported by the European Union's Horizon 2020 Research and Innovation Programme [grant agreement number 101004205].

Declaration of Competing Interest

The authors declare that they have no known competing financial interests or personal relationships that could have appeared to influence the work reported in this paper

Acknowledgments

The authors are very grateful to the colleagues at Exail for providing the sensors used during testing. The authors thank the EURISA (https://eurisa-h2020.eu/) consortium as a whole for the opportunity to work on such an interesting project.

Data availability

Data will be made available on request.

References

[1] T.R. Albrecht, P. Grütter, D. Horne, D. Rugar, Frequency modulation detection using high-Q cantilevers for enhanced force microscope sensitivity, J. Appl. Phys. 69 (1991) 668–673, https://doi.org/10.1063/1.347347.
[2] K.L. Ekinci, M.H. Huang, M.L. Roukes, Ultrasensitive nanoelectromechanical mass detection, Appl. Phys. Lett. 84 (2004) 4469–4471, https://doi.org/10.1063/1.1755417.
[3] T.A. Roessig, R.T. Howe, A.P. Pisano, J.H. Smith, Surface-Micromachined Resonant Accelerometer, IEEE 2, 1997, pp. 859–862, https://doi.org/10.1109/SENSOR.1997.635237.
[4] K. Tanaka, Y. Mochida, M. Sugimoto, K. Moriya, T. Hasegawa, K. Atsuchi, K. Ohwada, A micromachined vibrating gyroscope, Sens. Actuators A Phys. 50 (1995) 111–115, https://doi.org/10.1016/0924-4247(96)80093-8.
[5] K.M. Goeders, J.S. Colton, L.A. Bottomley, Microcantilevers: sensing chemical interactions via mechanical motion, Chem. Rev. 108 (2) (2008) 522–542, https://doi.org/10.1021/cr0681041.
[6] O. Le Traon, D. Janiaud, S. Muller, Monolithic accelerometric transducer, U.S. Patent No. 5,962,786, 1999. U.S. Patent and Trade-mark Office. ⟨https://image-ppubs.uspto.gov/dirsearch-public/print/downloadPdf/5962786⟩.
[7] O. Le Traon, D. Janiaud, S. Muller, P. Bouniol, The VIA Vibrating Beam Accelerometer: Concept and Performances, IEEE Position Locat., Palm Springs, United States of America, April 20–23, 1998. ⟨https://doi.org/10.1109/PLANS.1998.669865⟩.

[8] X.L. Feng, C.J. White, A. Hajimiri, M.L. Roukes, A self-sustaining ultrahigh-frequency nanoelectromechanical oscillator, Nat. Nanotechnol. 3 (2008) 342–346, https://doi.org/10.1038/nnano.2008.125.
[9] G. Sobreviela-Falces, M. Pandit, A. Mustafazade, C. Zhao, C. Pili, C. Baker, A. Seshia, A Mems Vibrating Beam Accelerometer for High Resolution Seismometry and Gravimetry, Proc. IEEE Micr. Elect., Gainesville, United States of America, January 25–29, 2021. ⟨https://doi.org/10.1109/MEMS51782.2021.9375431⟩.
[10] J.K. Sell, A.O. Niedermayer, B. Jakoby, A digital PLL circuit for resonator sensors, Sens. Actuators A Phys. 172 (2011) 69–74, https://doi.org/10.1016/j.sna.2011.02.030.
[11] J. Guérard, L. Delahaye, R. Levy, Digital electronics for inertial MEMS and space applications, Symposium on Design, Test, Integration & Packaging of MEMS and MOEMS (DTIP 2018), ROME, Italy, May, 2018. ⟨https://doi.org/10.1109/DTIP.2018.8394236⟩.
[12] O. Le Traon, J. Guérard, M. Pernice, C. Chartier, P. Lavenus, A. Andrieux, R. Levy, The NG DIVA: a Navigation Grade Differential Inertial Vibrating Beam Accelerometer, IEEE Position Locat., Monterey, United States of America, April 23–26, 2018. ⟨https://doi.org/10.1109/PLANS.2018.8373360⟩.
[13] G. Xia, Y. Zhao, Q. Shi, J. Huang, A. Qiu, A novel frequency readout method and circuit for navigation-grade vibrating beam accelerometers, IEEE Sens. J. 23 (18) (2023) 21363–21373, https://doi.org/10.1109/JSEN.2023.3300981.
[14] H. Besic, A. Demir, J. Steurer, N. Luhmann, S. Schmid, Schemes for tracking resonance frequency for micro- and nanomechanical resonators, Phys. Rev. Appl. 20 (2023), https://doi.org/10.1103/PhysRevApplied.20.024023.
[15] A. Demir, Understanding fundamental trade-offs in nanomechanical resonant sensors, J. Appl. Phys. 129 (2021) 044503, https://doi.org/10.1063/5.0035254.
[16] J.E.-Y. Lee, A.A. Seshia, Parasitic feedthrough cancellation techniques for enhanced electrical characterization of electrostatic microresonators, Sens. Actuators A Phys. 156 (2009) 36–42, https://doi.org/10.1016/j.sna.2009.02.005.
[17] V. Ferrari, D. Marioli, A. Taroni, Improving the Accuracy and Operating Range of Quartz Microbalance Sensors by A Purposely Designed Oscillator Circuit, IEEE IMTC P, Baltimore, United States of America2000, ⟨https://doi.org/10.1109/IMTC.2000.848670⟩.
[18] D.B. Leeson, A simple model of feedback oscillator noise spectrum, Proc. IEEE 54 (2) (1966) 329–330, https://doi.org/10.1109/PROC.1966.4682.
[19] O. Le Traon, D. Janiaud, M. Pernice, S. Masson, S. Muller, J.-Y. Tridera, A new quartz monolithic differential vibrating beam accelerometer, IEEE Position Locat. Corona USA (2006), https://doi.org/10.1109/PLANS.2006.1650581.

Didier Chérubin Negretto graduated from the Swiss Federal Institute of Technology in Lausanne, Switzerland with a specialisation in robotics in 2021. Since then he works for the Aerospace Electronics and Instrument Laboratory (AEIL) at the institute of geophysics, ETH Zurich, Switzerland as an electrical engineer.